

Lensless imaging by entangled photons from quadratic nonlinear photonic crystals

P. Xu,^{1,*} H. Y. Leng,¹ Z. H. Zhu,² Y. F. Bai,¹ H. Jin,¹ Y. X. Gong,^{1,3} X. Q. Yu,³ Z. D. Xie,¹ S. Y. Mu,¹ and S. N. Zhu¹

¹*National Laboratory of Solid State Microstructures and School of Physics, Nanjing University, Nanjing 210093, China*

²*College of Opto-Electronic Engineering, National University of Defense Technology, Changsha 410073, China*

³*Physics Department, Southeast University, Nanjing 211189, China*

(Received 10 August 2011; published 5 July 2012)

Lenses play a key role in quantum imaging but inevitably constrain the spatial resolution and working wavelength. In this work we develop and demonstrate a lensless quantum ghost imaging by engineering quadratic nonlinear photonic crystals. With a transverse parabolic domain modulation introduced into the lithium tantalate crystal, the entangled photon pairs generated from parametric down-conversion will self-focus. Therefore we can dispense with additional lenses to construct imaging in a nonlocal way. The lensless imaging is found to follow a specific imaging formula where the effective focal length is determined by the domain modulation and pump wavelength. Additionally, two nonlocal images can be retrieved when the entangled photon pair is generated under two concurrent noncollinear phase-matching geometries. Our work provides a principle and method to realize lensless ghost imaging, which may be extended to other wavelengths and stimulate new types of practical quantum technologies.

DOI: [10.1103/PhysRevA.86.013805](https://doi.org/10.1103/PhysRevA.86.013805)

PACS number(s): 42.50.Ar, 42.30.Va, 03.65.Ud, 42.65.Lm

I. INTRODUCTION

Developing advanced imaging techniques is of essential importance to human daily life and the scientific world. As one of the latest achievements of quantum mechanics, quantum imaging emerges with great advantages over the classical imaging. By using the quantum nature of entangled photons [1–8] or entangled beams [9–12], quantum imaging can surpass classical imaging with higher resolution and better sensitivity. In addition, quantum imaging is nonlocal. The image is constructed by joint detection between a beam that never interacts with the object and one that does. This ghost imaging was first demonstrated by using entangled photons in 1995 [1]. Since then, ghost imaging has drawn considerable attention due to its fundamental interest and potential applications. In practical implementations of quantum ghost imaging, the lens plays a key role in conveying the information from objects to images. But lenses severely constrain the spatial resolution and present engineering challenges at some wavelengths. Consequently, developing a lensless ghost imaging system is an important goal in quantum imaging science.

Here we develop and demonstrate lensless quantum imaging by engineering quadratic nonlinear photonic crystals (NPCs). The NPC offers high-efficiency nonlinear interactions in a quasi-phase-matching (QPM) way [13,14], and specifically a two-dimensional NPC [15,16] shows particular functionalities in the spatial control of second-harmonic beams [17–19] and entangled photons [20–22]. Very recently, a two-photon lens based on the transverse parabolic NPC was studied theoretically and experimentally [21,22]. In that case, the longitudinally periodic modulation of $\chi^{(2)}$ ensures the generation of entangled photon pairs by QPM spontaneously parametric down-conversion (SPDC), while in the transverse parabolic domain modulation, the crystal can tailor the wave front of the two photons, acting as an equivalent lens. In this work we investigate the two-photon lens and experimentally

demonstrate lensless quantum ghost imaging. The schematic layout for this lensless imaging is displayed in Fig. 1. When an object is put into one of the down-converted photon paths, by coincidence measurement the image can be reconstructed in the other down-converted path. No lens is required in this setup and even no beamsplitter is required when the signal and idler photon propagate noncollinearly. Furthermore, we obtain two lensless ghost images simultaneously under concurrent noncollinear QPM geometries in a multistriple parabolic NPC. This lensless quantum imaging presents a way to improve the resolution which is conventionally restricted by the size of lens, and offers a principle for engineering an equivalent lens by nonlinear interaction, hence it may be beneficial at frequencies where we do not have efficient ways of manufacturing lenses, such as x-rays.

The paper is organized as follows. Section II includes the mathematical description of the NPC's structure and theoretical calculations on the imaging formula for entangled photons from the NPC. In Sec. III, the experimental results of the single lensless ghost image and double lensless ghost images are given. In Sec. IV, the two-color lensless ghost imaging is discussed. The conclusion is drawn in Sec. V.

II. THEORETICAL CALCULATIONS ON THE IMAGING FORMULA

A. Description of the parabolic NPC

The quadratic nonlinear coefficient of parabolic NPC is expressed by

$$\chi^{(2)}(x, z) = d_{33} \text{sgn}\{\cos[2\pi(z + \alpha x^2)/\Lambda]\}, \quad (1)$$

which indicates the maximum nonlinear coefficient d_{33} is utilized and its sign changes when the domain is inverted. The longitudinal domain modulation period is Λ and the width of the positive domain is equal to that of the negative domain, while the transverse modulation follows the function $z = -\alpha x^2$. The Fourier expansion of $\chi^{(2)}(x, z)$ is $d_{33} \sum_n F(g_n) e^{ig_n(z + \alpha x^2)}$, where $g_n = n \frac{2\pi}{\Lambda}$ ($n = \pm 1, \pm 2, \dots$) represents the n th-order reciprocal vector and $F(g_n)$ is its

*pingxu520@nju.edu.cn

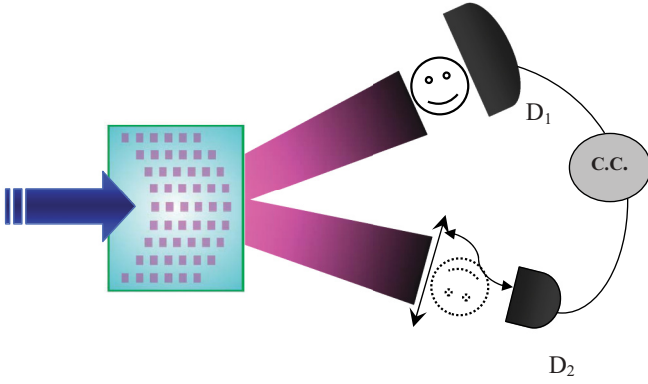


FIG. 1. (Color online) The schematic setup of lensless ghost imaging based on a multistripe parabolic NPC. The solid “face” represents the object and the dotted one represents the image.

corresponding Fourier coefficient. The entangled photons are generated under the QPM condition $k_p - k_s - k_i + g_n = 0$ along the propagation direction in which k_p , k_s , and k_i are wave vectors of the pump, signal, and idler, respectively. Along the x axis it is interesting to find that the wave front of entangled photon pairs takes a parabolic profile $e^{ig_n\alpha x^2}$. Hence the NPC is equivalent to a two-photon cylindrical lens [21].

In this work we design a multistripe parabolic NPC instead of a continuous one, as shown schematically in Fig. 1. The stripe interval is Λ_{tr} and the stripe width is $\Lambda_{tr}/2$. For each stripe, only its center follows $z = -\alpha x^2$. This design will bring new characters to the two-photon lens, such as the transverse periodicity and two lensless ghost images. The nonlinearity of a multistripe parabolic NPC is

$$\chi^{(2)}(x, z) = d_{33} \sum_n F(g_n) e^{ig_n z} \sum_m \text{rect}\left(\frac{x - m\Lambda_{tr}}{\Lambda_{tr}/2}\right) e^{ig_n\alpha(m\Lambda_{tr})^2}. \quad (2)$$

We define

$$U(x) = \sum_m \text{rect}\left(\frac{x - m\Lambda_{tr}}{\Lambda_{tr}/2}\right) e^{ig_n\alpha(m\Lambda_{tr})^2} \quad (3)$$

as the transverse structure function which includes both the amplitude and phase modulation. In this experiment we design the third-order reciprocal vector $g_{-3}(-g_3)$ to satisfy the quasi-phase-matching condition $k_p - k_s - k_i - g_3 = 0$. The effective two-photon wave front then takes the form of $e^{-ig_3\alpha(m\Lambda_{tr})^2}$. For deriving an analytical solution of two photons' spatial correlation, we use an approximated description of $U(x)$

$$U(x) = \sum_m \text{rect}\left(\frac{x - m\Lambda_{tr}}{\Lambda_{tr}/2}\right) e^{-ig_3\alpha x^2}, \quad (4)$$

where within each stripe the phase profile still follows the parabolic function $e^{-ig_3\alpha x^2}$ instead of the constant one $e^{-ig_3\alpha(m\Lambda_{tr})^2}$. It is worth noting that this approximation is reasonable since each stripe's width $\Lambda_{tr}/2$ is small and satisfies the far-field condition of $f_{\text{eff}} \gg (\Lambda_{tr}/2)^2/\lambda$ when the measurement is implemented in the two-photon focal plane $z = f_{\text{eff}}$ [23]. The Fourier expansion of $U(x)$ is $\frac{1}{2} \sum_m \sin c(m\pi/2) e^{i2\pi m x/\Lambda_{tr}} e^{-ig_3\alpha x^2}$ in which $\sin c(x) =$

$\frac{\sin(x)}{x}$. This form of $U(x)$ is convenient to use in the following calculations.

B. The imaging formula

Based on the first-order perturbation theory [24] and using the Hamiltonian $H_I = \varepsilon_0 \int_V d\vec{r} \chi^{(2)}(x, z) \{E_p^{(+)} E_s^{(-)} E_i^{(-)}\} + \text{H.c.}$, we obtain the two-photon state

$$|\psi\rangle \propto \psi_0 \sum_{\vec{k}_s, \vec{k}_i} H_{tr}(\vec{k}_s, \vec{k}_i) \hat{a}^{(+)}(\vec{k}_s) \hat{a}_i^{(+)}(\vec{k}_i) |0\rangle, \quad (5)$$

in which all the slowly varying terms and constants are absorbed into ψ_0 . \vec{k}_s, \vec{k}_i are the transverse wave vectors of signal and idler photons, respectively. Here we assume the frequency mode function and spatial mode function of the two-photon state factor and are only concerned with the transverse part [24]. The transverse two-photon mode function is calculated as

$$H_{tr}(\vec{k}_s, \vec{k}_i) = \int d\vec{\rho} \{U(\vec{\rho}) E(\vec{\rho})\} e^{-i(\vec{k}_s + \vec{k}_i) \cdot \vec{\rho}}, \quad (6)$$

in which $E(\vec{\rho})$ is the pump beam's profile and $U(\vec{\rho})$ represents the two-dimensional structure function of the NPC. Since the state-of-the-art crystal poling technique only enables two-dimensional domain engineering, the domain modulation along the y axis is homogenous. For the plane-wave pump, the mode function along the y axis is given by $H_{tr}(\kappa_{sy}, \kappa_{iy}) = \int dy e^{-i(\kappa_{sy} + \kappa_{iy})y} \propto \delta(\kappa_{sy} + \kappa_{iy})$, while the mode function along the x axis is $H_{tr}(\kappa_{sx}, \kappa_{ix}) = \int dx U(x) e^{-i(\kappa_{sx} + \kappa_{ix})x} \propto \sum_m \sin c\left(\frac{m\pi}{2}\right) \int d\kappa \delta(\kappa_{sx} + \kappa_{ix} - \kappa - \frac{2\pi m}{\Lambda_{tr}}) e^{i\frac{\kappa^2}{4g_3\alpha}}$. In the following part, we will only be concerned with the spatial correlation along the x axis.

Suppose signal and idler photons are captured by detector D_1 and D_2 , respectively. $E_j^{(+)}(\vec{r}_j, t_j)$ is the electromagnetic field evaluated at the two detectors' spatial coordinate $\vec{r}_j(\vec{\rho}_j, z_j)$ ($j = s, i$). z_s and z_i stand for the distance from the crystal to the object and the imaging plane, respectively. The propagation of the two free-space electromagnetic fields is $E_j^{(+)}(\vec{r}_j, t_j) = \sum_{\vec{k}_j} E_j e^{-i\omega_j t_j} g(\vec{k}_j, \omega_j; \vec{\rho}_j, z_j) \hat{a}_{\vec{k}_j}$, in which Green's function takes the form of $g(\vec{k}_j, \omega_j; \vec{\rho}_j, z_j) = \frac{e^{i\vec{k}_j \cdot \vec{z}_j}}{i\lambda_j z_j} \int d\vec{\rho}_s e^{i\frac{\omega_j}{2cz_i} |\vec{\rho}_j - \vec{\rho}_s|^2} e^{i\vec{k}_j \cdot \vec{\rho}_s}$ [24]. Suppose the transverse component is smaller and satisfies $|\vec{k}_j| \ll |\vec{k}_j|$, then we have $\vec{k}_j = |\vec{k}_j| \hat{e}_z + \vec{k}_j$. Two-photon amplitude $A(x_s, x_i) = \langle 0 | E_2^{(+)} E_1^{(+)} | \psi \rangle$ is calculated to be

$$A(x_s, x_i) \propto \int dx E(x) \sum_m \sin c(m\pi/2) e^{i2\pi m x/\Lambda_{tr}} \times e^{i\left(\frac{\omega_s x_s}{2cz_s} + \frac{\omega_i x_i}{2cz_i} - g_3\alpha\right)x^2} e^{-i\left(\frac{\omega_s x_s}{cz_s} + \frac{\omega_i x_i}{cz_i}\right)x}. \quad (7)$$

When taking the pump to be transversely infinite, we obtain a point-to-point correspondence along the x axis between the signal and idler photon

$$G^{(2)}(x_s, x_i) = |A(x_s, x_i)|^2 \propto \left| \sum_m \sin c\left(\frac{m\pi}{2}\right) \times \delta\left(\frac{\omega_s x_s}{cz_s} + \frac{\omega_i x_i}{cz_i} - \frac{2\pi m}{\Lambda_{tr}}\right) \right|^2, \quad (8)$$

under the condition of $\frac{\omega_s}{2cz_s} + \frac{\omega_i}{2cz_i} - g_3\alpha = 0$. Thus the imaging formula is obtained and it can be written as

$$\frac{1}{\lambda_s z_s} + \frac{1}{\lambda_i z_i} = \frac{1}{\lambda_p f_{\text{eff}}}, \quad (9)$$

in which f_{eff} equals $\frac{\pi}{g_3\alpha\lambda_p}$. So f_{eff} is relevant to the pump wavelength, the curvature of the parabolic NPC, and the reciprocal vector for the longitudinal quasi-phase-matching condition. The two-photon wave front takes another form of $\varphi(x) = e^{-ig_3\alpha x^2} = e^{-ik_p x^2/2f_{\text{eff}}}$. If one uses a point detector to scan and detect two-photon probability after the crystal, two-photon focusing as well as the far-field diffraction of the multistripe will be observed at the plane $z = f_{\text{eff}}$ [22], thus multiple focal spots may be observed. When one puts an object in one of the paths, the image will be recovered in the other path by coincidence measurement. The image is linearly magnified by a factor of $-\frac{\lambda_i z_i}{\lambda_s z_s}$ when the object is put into the signal path. For degenerate photon pair generation, the imaging formula will be simplified to $\frac{1}{z_s} + \frac{1}{z_i} = \frac{2}{f_{\text{eff}}}$. If we set $z_s = z_i = f_{\text{eff}}$, an equal-size reproduction of the object will be retrieved. According to Eq. (8), there should be many equally spaced ghost images and the intensity of high-order images are decided by the $\sin c$ function. However, the number of observable ghost images should be further limited by the single-photon distribution.

Consider a pump with a Gaussian spatial profile with beam waist w_0 , the spatial correspondence of photon pair will take the form

$$G^{(2)}(x_s, x_i) \propto \left| \sum_m \sin c\left(\frac{m\pi}{2}\right) e^{-\pi^2\left(\frac{x_s}{\lambda_s z_s} + \frac{x_i}{\lambda_i z_i} - \frac{m}{\Lambda_{tr}}\right)^2 w_0^2} \right|^2. \quad (10)$$

For a zero-order ghost image, i.e., $m = 0$, the imaging resolution is $\lambda_i z_i / w_0 \pi$ when the object is put in the signal path.

III. EXPERIMENTAL RESULTS OF LENSLESS GHOST IMAGING

A. Single lensless ghost image

In this experiment we engineer the multistripe ferroelectric domains in LiTaO₃ as Fig. 2(a) shows. The longitudinal periodicity of NPC is $\Lambda = 13.917 \mu\text{m}$, which ensures efficient entangled photon generation with the third-order reciprocal vector $g_3 = 3(2\pi)/\Lambda$. The transverse modulation follows $z = -\alpha x^2$ and $\alpha = 15.226 \text{ m}^{-1}$. It indicates that $f_{\text{eff}} = 33.3 \text{ mm}$ when the crystal is pumped by 457 nm. The stripe interval Λ_{tr} is $20 \mu\text{m}$, stripe width b is $10 \mu\text{m}$, and stripe length L is 6 mm . The crystal is pumped with a cw single longitudinal mode 457-nm laser and embedded in an oven for temperature control to produce the degenerate photon pairs at 914 nm. M_1 reflects the pump and keeps the entangled photons transmitted. M_2 is a beamsplitter. A bucket detector D_1 is put in the signal path and collects all the photons after the object which is a double slit aperture with slit width $150 \mu\text{m}$ and slit separation $300 \mu\text{m}$. For the transmitted path, the fiber tip scans along the direction of x axis and it is followed by another single-photon detector D_2 . Two bandpass filters IF_1 and IF_2 with 10-nm FWHM are put before two single-photon

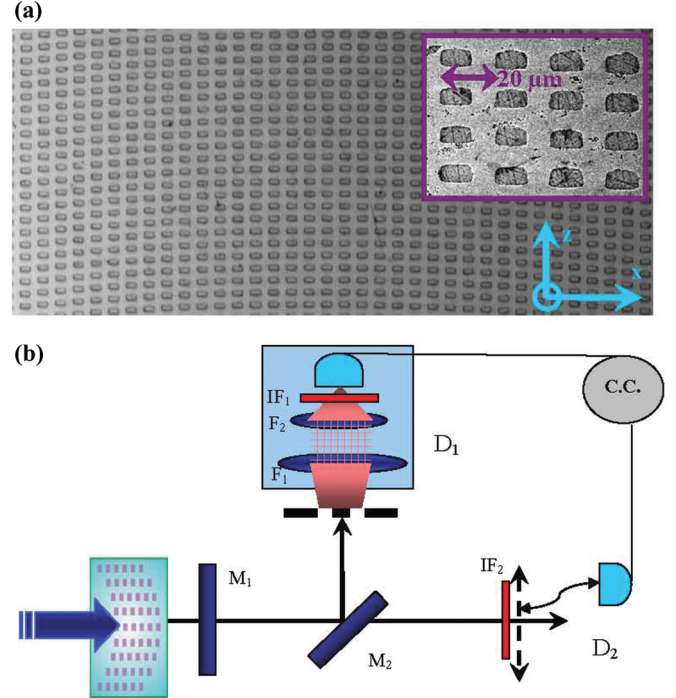


FIG. 2. (Color online) Photograph of NPC sample (a) and experimental setup (b). The bucket detector D_1 consists of two collection lenses and a single-photon detector. It collects all the photons after the double slit.

detectors to further suppress the pump. No additional imaging lens is required in this imaging setup.

When the working temperature of the NPC is set at 180.1°C and the pump is incident along its center, degenerate entangled photon pairs are generated collinearly; the two-dimensional single-photon counting profile at D_2 is presented in Fig. 3(a). When making coincidence counting between two detectors, a clear image of the double slit appears as in Fig. 3(b). When we set the object distance $z_s = 33.3 \text{ mm}$, the ghost image plane is found to be located at around $z_i = 32.4 \text{ mm}$. The measured separation of the double slit is $303 \mu\text{m}$, and a Gaussian fitting of the peaks gives slit widths (FWHM) of 146 and $142 \mu\text{m}$, respectively. Hence a nearly equal-size image is obtained. When the scanning fiber tip locates out-of-focus, the image gets blurred. A preliminary test for the spatial resolution gives $33 \mu\text{m}$ (FWHM) by using the single-mode fiber tip as the object, while the theoretical value is $28 \mu\text{m}$ with a full pump width of 0.82 mm . Since no additional imaging lens is used in this experiment, the imaging resolution is determined only by the pump size and wavelength of the entangled photons. As we have calculated, the photon pair emerges from the same point of crystal and each photon pair takes all the possible combinations of momentum with a certain phase distribution which results from the transverse parabolic modulation. This lensless ghost imaging can be explained through analogies to geometric optics. Figure 3(c) is an unfolded layout of the lensless imaging. The geometric ray in Fig. 3(c) actually represents the two-photon amplitude. The superposition of these two-photon amplitudes builds up a nonlocal point-to-point correspondence between the signal and idler path. The parabolic NPC works equivalently as

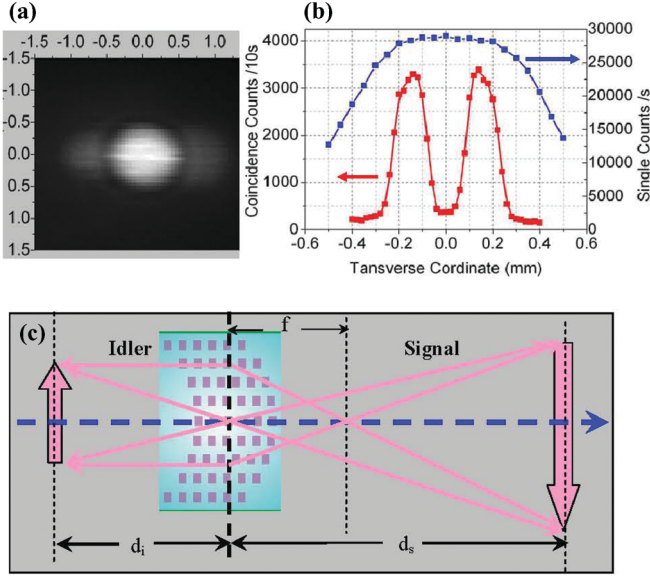


FIG. 3. (Color online) (a) Single-photon profile at D₂. (b) Single-photon counting distribution is denoted by the upper blue symbols and the coincidence counting by the lower red symbols. The bucket detector D₁ gives the photon counting rate 0.25 Mc/s and the maximum coincidence counting rate is 330 c/s. (c) The unfolded layout of lensless ghost imaging.

the imaging lens. The spatial resolution of such lensless imaging is the same as the ghost imaging implemented with a homogeneous bulk nonlinear optical crystal and a cylindrical lens with a large enough aperture under the same experiment configuration including the wavelength of entangled photons, the crystal size, and the image distance. Here, we have to emphasize that higher order ghost images are not observed since the spatial interval of two adjacent ghost images is beyond the single-photon distribution as shown in Fig. 3(a).

B. Double lensless ghost images

As first considered in Ref. [21], the alignment of the multiple stripes transforms the two-photon spatial entanglement and brings new characters. Here for the multistripe parabolic NPC sample described by Eq. (3), we find the structure function $U(x)$ reproduces itself after a translation of $d = \frac{\lambda_p f_{\text{eff}}}{\Lambda_{tr}}$ which indicates our crystal structure has a translational periodicity:

$$\begin{aligned}
 U\left(x - \frac{\lambda_p f_{\text{eff}}}{\Lambda_{tr}}\right) &= \sum_m \text{rect}\left(\frac{x - \lambda_p f_{\text{eff}}/\Lambda_{tr} - m\Lambda_{tr}}{\Lambda_{tr}/2}\right) e^{-ig_3\alpha(m\Lambda_{tr})^2} \\
 &= \sum_m \text{rect}\left(\frac{x - m'\Lambda_{tr}}{\Lambda_{tr}/2}\right) e^{-ig_3\alpha(m'\Lambda_{tr})^2} = U(x), \quad (11)
 \end{aligned}$$

where we have used relations $g_3\alpha = \frac{\pi}{\lambda_p f_{\text{eff}}}$, $\frac{\lambda_p f_{\text{eff}}}{\Lambda_{tr}} = 38.08\Lambda_{tr} \approx 38\Lambda_{tr}$, and $m' = m + \frac{\lambda_p f_{\text{eff}}}{\Lambda_{tr}^2} \approx m + 38$. Therefore when the crystal is translated by a distance of $j\lambda_p f_{\text{eff}}/\Lambda_{tr}$ ($j = 0, \pm 1, \pm 2, \dots$), both the image positions and the image intensity remain the same. The crystal works as a two-photon lens which has multiple equally spaced principal axes on it. All

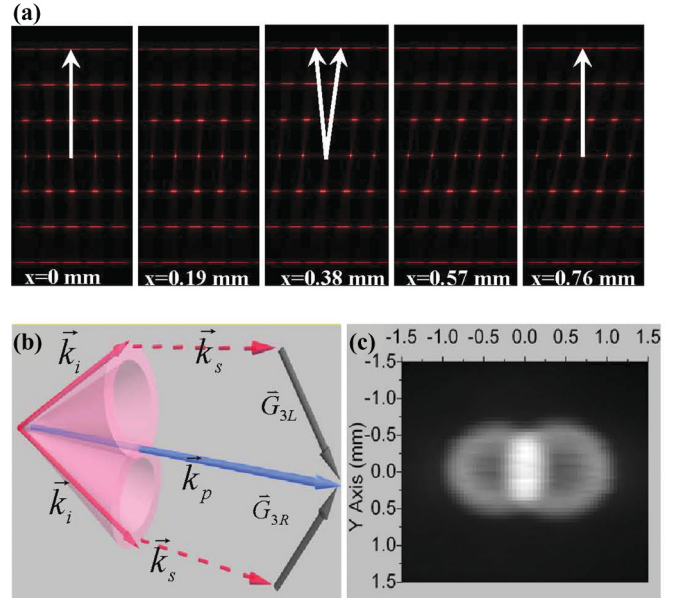


FIG. 4. (Color online) (a) Theoretical Fourier spectra of NPC when the pump is incident on different positions of NPC. (b) The corresponding QPM geometry for two single-photon cones. Each cone is quasi-phase-matched by a tilted reciprocal vector \vec{g}_{3L} or \vec{g}_{3R} and the cone axis is along $\vec{k}_p - \vec{g}_{3L}$ or $\vec{k}_p - \vec{g}_{3R}$. (c) The measured single-photon distribution.

these principal axes are equivalent so that when the incident pump lies halfway between two principal axes, the two images near the center will have equivalent intensities.

Experimentally we found that the single-photon distribution and ghost imaging can be recovered when the crystal shifts by multiples of $\lambda_p f_{\text{eff}}/\Lambda_{tr}$ (0.76 mm), which consists well with the above theoretical calculation. This transverse periodicity can also be understood from the viewpoint of reciprocal space of such NPCs. Figure 4(a) is the theoretical simulation about the reciprocal space of the crystal by Fourier transformation when the pump is incident on different positions of the crystal. The reciprocal space is distorted when the pump moves away from the central position and it will recover when the pump moves 0.76 mm away. When the pump is incident in between, i.e., $x = 0.38$ mm, from the reciprocal space we can see that two noncollinear reciprocal vectors \vec{g}_{3L} and \vec{g}_{3R} with mirror symmetry exist, which may work for new types of entangled photon generation under $\vec{k}_s + \vec{k}_i + \vec{g}_{3L(3R)} = \vec{k}_p$. For a two-dimensional NPC without parabolic modulation, the classical parametric down-conversion process participant by such a pair of reciprocal vectors has been reported [25,26]. For the spontaneous parametric down-conversion in this parabolic NPC sample, the QPM geometry is similar. The only difference is that the photon pair carries a parabolic phase profile. Figure 4(b) shows two concurrent noncollinear QPM geometries which result in two tangent single-photon cones. If one takes the advantage of concurrent QPMs in the NPC sample, multiple images can be obtained.

In the experiment, when the crystal moves 0.38 mm away from the center and the temperature is tuned to 178.5 °C, two tangent single-photon rings are captured, as shown in Fig. 4(c). So when the signal photon travels along the pump direction, the

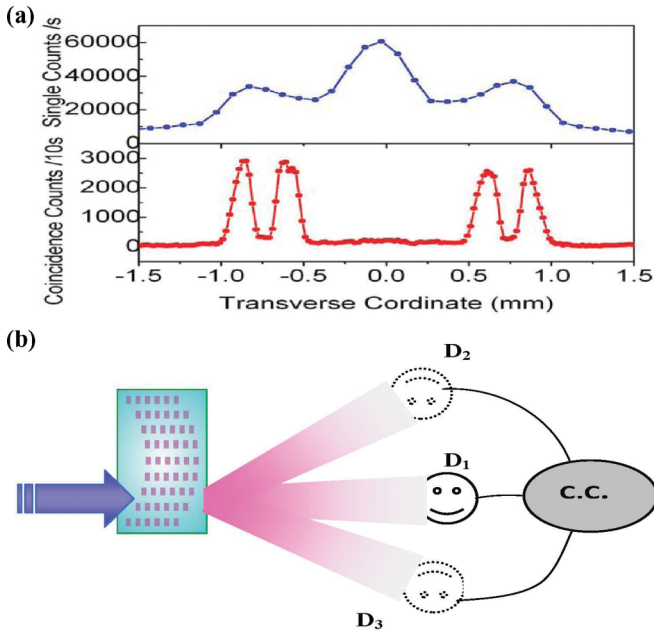


FIG. 5. (Color online) (a) Two ghost images of double slit whose size is close to that of the object mask. (b) The schematic layout for simultaneous construction of two ghost images. The single photon detector D_1 in the object path is a bucket detector whose combination is similar to that in Fig. 2(b). Single-photon detectors D_2 and D_3 are spatially resolving.

idler will emerge from either ring indistinguishably. If we put the object into the overlap region of the two rings, two ghost images will be expected at the outer sides of two single-photon rings. Figure 5(a) shows the experimental results under the same experimental configuration as in Fig. 2(b). Two equal-size images of double slit are obtained in the transmitted path when the fiber tip is scanning in the in-focus plane. The experimental setup can be further simplified into Fig. 5(b). No beamsplitter is required since the photon pair is naturally separated. Such concurrent ghost images may also be realized by the homogenous bulk nonlinear crystal; however, additional optical elements including a lens and beamsplitter are required.

IV. DISCUSSIONS

Since quasi-phase-matching generation of entangled photons enriches the range of working wavelengths, with nonde-

generate photon pairs we may achieve a two-color lensless ghost imaging. The resolving power and field of view can be greatly enhanced [6] when the photons in the spatially resolved path have much higher frequency. Also the wavelengths of the photon pair can be designed according to practical use such as the midinfrared, fiber communication wavelength, or nondestructive wavelength for observing biological samples. Besides, the resolution of the lensless imaging can be further improved through increasing the pump size and engineering a continuous parabolic NPC. But we have to emphasize that the lensless imaging demonstrated in this work is one-dimensional, and the two-dimensional one relies on the fabrication of three-dimensional NPCs.

V. CONCLUSIONS

The lensless quantum imaging demonstrated in this work is performed by the momentum correlation manipulation of the entangled two-photon pair by engineering nonlinear photonic crystals. The engineering of spatial entanglement helps us explore fundamental concerns in quantum mechanics and practical quantum technologies such as the lensless quantum imaging described in this work. The lensless imaging offers a principle for engineering equivalent lenses during the nonlinear interaction and opens a door for lensless imaging at specific regions of the electromagnetic spectrum like x-rays [27], terahertz, infrared, microwave radiation, as well as acoustic wave. Preparing other new types of entangled states with tailored mode functions and the extension to entangled bright beams from high-gain parametric down-conversion deserves further investigation.

ACKNOWLEDGMENTS

The authors thank Y. H. Shih for valuable discussions and Q. J. Wang for evaluating the quality of the sample. This work was supported by the State Key Program for Basic Research of China (No. 2012CB921802 and No. 2011CBA00205), the National Natural Science Foundations of China (No. 11174121, No. 91121001, and No. 11021403), the Project Funded by the Priority Academic Program Development of Jiangsu Higher Education Institutions (PAPD), and the Foundation for the Author of National Excellent Doctoral Dissertation of PR China (FANEDD).

-
- [1] T. B. Pittman, Y. H. Shih, D. V. Strekalov, and A. V. Sergienko, *Phys. Rev. A* **52**, R3429 (1995).
 - [2] T. B. Pittman, D. V. Strekalov, D. N. Klyshko, M. H. Rubin, A. V. Sergienko, and Y. H. Shih, *Phys. Rev. A* **53**, 2804 (1996).
 - [3] A. F. Abouraddy, B. E. A. Saleh, A. V. Sergienko, and M. C. Teich, *Phys. Rev. Lett.* **87**, 123602 (2001).
 - [4] A. F. Abouraddy, B. E. A. Saleh, A. V. Sergienko, and M. C. Teich, *J. Opt. Soc. Am. B* **19**, 1174 (2002).
 - [5] M. D'Angelo, Y. H. Kim, S. P. Kulik, and Y. H. Shih, *Phys. Rev. Lett.* **92**, 233601 (2004).
 - [6] M. H. Rubin and Y. H. Shih, *Phys. Rev. A* **78**, 033836 (2008).
 - [7] M. Malik, H. Shin, M. O'Sullivan, P. Zerom, and R. W. Boyd, *Phys. Rev. Lett.* **104**, 163602 (2010).
 - [8] B. Jack, J. Leach, J. Romero, S. Franke-Arnold, M. Ritsch-Marte, S. M. Barnett, and M. J. Padgett, *Phys. Rev. Lett.* **103**, 083602 (2009).
 - [9] M. I. Kolobov, *Rev. Mod. Phys.* **71**, 1539 (1999).
 - [10] A. Gatti, E. Brambilla, and L. A. Lugiato, *Phys. Rev. Lett.* **90**, 133603 (2003).

- [11] G. Brida, M. Genovese, and I. Ruo Berchera, *Nature Photonics* **4**, 227 (2010).
- [12] V. Boyer, A. M. Marino, R. C. Pooser, and P. D. Lett, *Science* **321**, 544 (2008).
- [13] J. A. Armstrong, N. Bloembergen, J. Ducuing, and P. S. Pershan, *Phys. Rev.* **127**, 1918 (1962).
- [14] P. A. Franken and J. F. Ward, *Rev. Mod. Phys.* **35**, 23 (1963).
- [15] V. Berger, *Phys. Rev. Lett.* **81**, 4136 (1998).
- [16] N. G. R. Broderick, G. W. Ross, H. L. Offerhaus, D. J. Richardson, and D. C. Hanna, *Phys. Rev. Lett.* **84**, 4345 (2000).
- [17] J. R. Kurz, A. M. Schober, D. S. Hum, A. J. Saltzman, and M. M. Fejer, *IEEE J. Sel. Top. Quantum Electron.* **8**, 660 (2002).
- [18] Y. Q. Qin, C. Zhang, Y. Y. Zhu, X. P. Hu, and G. Zhao, *Phys. Rev. Lett.* **100**, 063902 (2008).
- [19] T. Ellenbogen, N. Voloch-Bloch, A. Ganany-Padowicz, and A. Arie, *Nat. Photon.* **3**, 395 (2009).
- [20] X. Q. Yu, P. Xu, Z. D. Xie, J. F. Wang, H. Y. Leng, J. S. Zhao, S. N. Zhu, and N. B. Ming, *Phys. Rev. Lett.* **101**, 233601 (2008).
- [21] J. P. Torres, A. Alexandrescu, S. Carrasco, and L. Torner, *Opt. Lett.* **29**, 376 (2004).
- [22] H. Y. Leng, X. Q. Yu, Y. X. Gong, P. Xu, Z. D. Xie, H. Jin, C. Zhang, and S. N. Zhu, *Nature Commun.* **2**, 429 (2011).
- [23] When this far-field condition is satisfied, we will ignore the propagation phase difference within each stripe and only be concerned with the initial phase of the photon pair then integrate over the stripe. For the stripe centered at $x_0 = m\Lambda_{tr}$, the integration over the m th stripe gives $E_m = \int_{x_0 - \Lambda_{tr}/4}^{x_0 + \Lambda_{tr}/4} e^{ig_n \alpha x_0^2} dx$ for the flat stripe and $E'_m = \int_{x_0 - \Lambda_{tr}/4}^{x_0 + \Lambda_{tr}/4} e^{ig_n \alpha x^2} dx$ for the parabolic stripe. Under the condition of $g_n \alpha (\Lambda_{tr}/4)^2 \ll 1$, we will derive $E_m = E'_m / \sin c(g_n \alpha x_0 \Lambda_{tr}/2)$ in which $\sin c(g_n \alpha x_0 \Lambda_{tr}/2) \approx 1$ for any stripe within the pump beamwidth. So the approximation in Eq. (4) is reasonable and it will not affect the focal spot size and focal length of such two-photon lenses.
- [24] M. H. Rubin, *Phys. Rev. A* **54**, 5349 (1996).
- [25] H.-C. Liu and A. H. Kung, *Opt. Express* **16**, 9714 (2008).
- [26] K. Gallo, M. Levenius, F. Laurell, and V. Pasiskevicius, *Appl. Phys. Lett.* **98**, 161113 (2011).
- [27] S. Shwartz and S. E. Harris, *Phys. Rev. Lett.* **106**, 080501 (2011).